

# Simulations of Grain Growth in Titanium and Stainless Steels

Akira SEKI\*  
Koji MORIGUCHI

Masayoshi SAWADA  
Yoshihisa SHIRAI

## Abstract

*Grain growth simulations of titanium and stainless steels have been performed using phase-field model. In the simulation of Ti-rich Ti-Fe-O ternary alloys modeling commercially pure titanium, it was shown that a grain growth is suppressed by the pinning effect by  $\beta$  grains in thermal equilibrium. In the mesoscopic grain growth simulation of SUS301L austenitic stainless steel alloyed with Nb, where the pinning effect of Nb (C, N) is described by one pinning parameter, the average size of Nb (C, N) particles was estimated. The calculated grain sizes obtained by the simulations of the titanium alloy and the stainless steels agree well with experimental grain sizes.*

## 1. Introduction

As in the case of other metallic materials, the mechanical properties of commercially pure titanium and titanium alloys for industrial use (hereinafter, “titanium”) and of stainless steels are largely influenced by their grain sizes.<sup>1-3)</sup> Therefore, one of the purposes of microstructure control<sup>4)</sup> of titanium or stainless steel is to control its grain size. To that end, it is necessary to optimize the manufacturing conditions for the material.

In recent years, attention has been paid to microstructure prediction using the phase-field model<sup>5,6)</sup> or some other simulation technique.<sup>6)</sup> We are making various attempts to predict the microstructures of titanium and stainless steels. One example is simulating the growth of grains to estimate grain size.

The Monte Carlo method and the cellular automaton method are known to be effective in simulating the growth of grains.<sup>6)</sup> The algorithm of each of these methods has been so constructed as to produce the Gibbs–Thomson effect. The Monte Carlo method is a purely probabilistic technique, whereas the cellular automaton method is a technique that contains a probabilistic aspect. Despite the fact that the two methods are simple and easy, they reproduce the observed microstructure to a good extent. In recent years, in addition to those probabilistic techniques, the phase-field model has come to be used in grain growth simulations.<sup>7-9)</sup>

The phase-field model or multiphase-field model<sup>10)</sup> can easily be coupled with CALPHAD<sup>11)</sup> that is a free energy calculation model. In addition, the method contains a description of substance transport in its framework. In the present study, to simulate the growth of grains, while also taking into consideration the alloy composition

and impurities, through thermodynamic calculations of the phase stability, and paying due attention to the substance transport, we decided to employ the multiphase-field model to carry out the simulations. This paper presents two examples of grain growth simulations with titanium and stainless steel. In each example, the accuracy of simulation was checked by comparing the simulation results with the results of an experiment carried out concurrently.

## 2. Multiphase-Field Model

In the present study, we used a two-dimensional (2D) multiphase-field model. In this model, a phase field is given to each of the grains. Note that the grains may have different phases (Fig. 1). The equation of evolution of phase field  $\phi_p$  formulated by Eiken et al.<sup>12)</sup> is shown below.

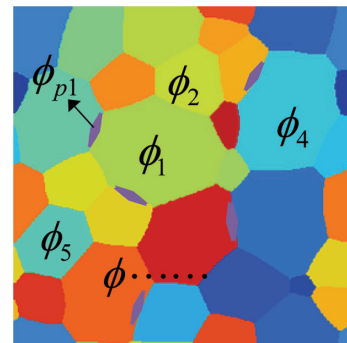


Fig. 1 Grain structure where phase-field is defined for each grain

\* Senior Researcher, Dr.Eng., Titanium & Specialty Stainless Steel Research Lab., Steel Research Laboratories  
1-8 Fuso-cho, Amagasaki City, Hyogo Pref. 660-0891

$$\frac{d\phi_p}{dt} = \sum_{q=1}^v \frac{M_{pq}}{V} \left\{ \sum_{r=1}^v \left[ (\sigma_{qr} - \sigma_{pr}) \left( \frac{\pi^2}{\eta^2} \phi_r + \nabla^2 \phi_r \right) \right] + \frac{2\pi}{\eta} \sqrt{\phi_p \phi_q} \Delta g_{pq} \right\}, \quad (1)$$

where the value of  $v$  is an integer 1, 2, or 3 depending on bulk, interfacial region, etc.;  $M_{pq}$ , the mobility of interface  $p/q$ ;  $\sigma_{pq}$ , the interfacial energy of  $p$  and  $q$  grains; and  $\Delta g_{pq}$ , the driving force for transformation between  $p$  and  $q$ .  $\eta$  denotes the ‘‘interface width’’ set for the purpose of numerical calculations. It was decided to be five times of the mesh for numerical calculations.

The above evolution equation (1) describes not only such structural changes as solidification and phase transformation induced by a thermodynamic driving force but also the growth of grains determined by grain boundary curvature and grain boundary energy. Namely, Equation (1) includes driving force  $\Delta G$  for grain growth by the Gibbs–Thomson effect<sup>13)</sup> expressed by the following equation.

$$\Delta G = \frac{2\sigma}{R}, \quad (2)$$

where  $R$  denotes the radius of curvature of grains.

The driving force for transformation,  $\Delta g_{pq}$ , can be calculated by using a database for the actual material by means of the coupling with a Thermo-Calc<sup>14)</sup> calculation, for example. Namely, since the equation permits using an existing database for multicomponent materials, it can be applied even to practical multicomponent materials, such as titanium and stainless steel.

Although grain boundary mobility  $M$  is often used as the fitting parameter for experimental values of interface motion, a model expressed by the following equation is available for  $M$ .<sup>13, 15)</sup>

$$M \approx \frac{V \cdot D_{gb}}{\delta RT} = \frac{V}{\delta RT} D_0 \exp\left(-\frac{Q}{RT}\right), \quad (3)$$

where  $V$ ,  $\delta$ , and  $D_{gb}$  denote molar volume, grain boundary width, and grain boundary diffusion coefficient, respectively.

In the multiphase-field method, it is possible to couple solute atom transport equations (diffusion equations). The following equation is a transport equation derived from the diffusion equation of an impure element by Tiaeden et al.<sup>16)</sup>

$$\frac{\partial c_i(\mathbf{r}, t)}{\partial t} = \nabla \cdot \sum_p \phi_p D_i^p \nabla c_i^p(\mathbf{r}, t), \quad c_i(\mathbf{r}, t) = \sum_p \phi_p c_i^p(\mathbf{r}, t), \quad (4)$$

where  $c_i(\mathbf{r}, t)$  denotes the concentration of solute element  $i$  and  $c_i^p(\mathbf{r}, t)$  denotes the solute element concentration within the  $p$  phase.  $D_i^p$  is the diffusion coefficient of solute  $i$  in the  $p$  phase. By performing a numerical calculation with a thermodynamic calculation coupled with Equations (1) and (4), the evolution of microstructure can be calculated and visualized two-dimensionally.

### 3. Grain Growth in Titanium

We simulated the growth of grains in commercially pure titanium sheets. In many cases, they are manufactured and used in an  $\alpha$ -phase region. The primary purpose of microstructure control is to control the size of  $\alpha$  grains. The desired  $\alpha$ -grain size can be obtained by adjusting properly the heat treatment temperature and time. Fe added to the sheet together with oxygen for increasing the sheet strength is an element which helps stabilize  $\beta$  phase. Therefore, as the amount of Fe addition is increased, the ( $\alpha + \beta$ ) dual phase region expands. Since it was considered that the  $\beta$  phase would influence the growth of  $\alpha$  grains, we carried out a simulation taking Fe and oxygen into account and studied the growth behavior of  $\alpha$  grains in

**Table 1** Chemical compositions of samples used for the grain growth experiments of commercially pure titanium

Sample	Fe	O	Ti	Volume % of $\beta$ phase at 800°C (Thermo-Calc)
Material A	0.03	0.05	Balance	0
Material B	0.07	0.07	Balance	1

the presence of  $\beta$  phase. In the simulation, multiphase field software<sup>17)</sup> of our own making was used.

#### 3.1 Experimental

Two types of commercially pure titanium were subjected to an experiment. Their chemical compositions are shown in **Table 1**. Each of the samples was prepared by subjecting a hot-rolled sheet first to solution heat treatment of  $\alpha$  phase at 700°C  $\times$  30 min and then to 60% cold working and final heat treatment at 800°C for up to 600 s. The final heat treatment represents the process of grain growth. The microstructure of Sample A observed under an optical microscope was entirely of  $\alpha$  phase. On the other hand, Sample B revealed a second phase considered  $\beta$  phase. Table 1 also shows the volume % of  $\beta$  phase in equilibrium state at 800°C calculated by Thermo-Calc. The calculated value coincides with the result of observation of the microstructure. The grain size in terms of grain diameter was calculated from the number of grains counted in a certain region of a photograph of the microstructure obtained by an optical microscope.

#### 3.2 Method of simulation

By coupling Equations (1) and (4), we carried out a simulation taking into account the  $\alpha/\beta$  phase transformation and the transport of Fe and oxygen. The driving force for the  $\alpha/\beta$  phase transformation was calculated through the coupling with Thermo-Calc using the TQ-Interface.<sup>14)</sup> The thermodynamic database used was Ti3.

The chemical compositions of the model materials are the same as those of the samples used in the experiment (Table 1). The calculation region was 400  $\mu\text{m} \times$  400  $\mu\text{m}$ . The mesh size was 0.5  $\mu\text{m}$  and the number of meshes was 800  $\times$  800. To eliminate the influence of the edges of the calculation region, periodic boundary conditions were adopted. Values given in the reference<sup>18)</sup> were used as the diffusion coefficients of Fe and oxygen in  $\alpha$  and  $\beta$  phases, respectively. The interfacial energies,  $\sigma_{\alpha\alpha}$  and  $\sigma_{\alpha\beta}$ , were each assumed to be 1 J/m<sup>2</sup>. The grain boundary mobility of  $\alpha$  grains,  $M_{\alpha\alpha}$ , was used as the fitting parameter, and the mobility of interface between different phases,  $M_{\alpha\beta}$ , was assumed to be  $M_{\alpha\alpha}/5$ .

#### 3.3 Growth of grains in $\alpha$ phase region

Material A that was entirely of  $\alpha$  phase at 800°C was subjected to the above simulation to obtain the mobility of  $\alpha$  grain boundary. The simulation was carried out with the initial microstructure and  $\alpha$ -grain boundary mobility  $M_{\alpha\alpha}$  varied such that the temporal evolution of average grain size would agree with the experimental result. The simulation results are shown in **Fig. 2**. When  $M_{\alpha\alpha} = 6 \times 10^{-12}$  m<sup>4</sup>/Js, the simulation results agree fairly well with the experimental results. Therefore, this value is assumed to be the  $\alpha$ -grain boundary mobility at 800°C. **Figure 3** shows the experimental microstructures associated with the microstructures of Material A simulated when the above grain boundary mobility was used.

#### 3.4 Growth of grains in ( $\alpha + \beta$ ) dual phase region

At 800°C, Material B contains  $\beta$  phase and hence becomes  $\alpha + \beta$  dual phase. Since it was necessary to consider the distribution of Fe and oxygen between  $\alpha$  and  $\beta$  phases and the transformation between  $\alpha$  and  $\beta$  phases, we coupled diffusion calculation and phase transfor-

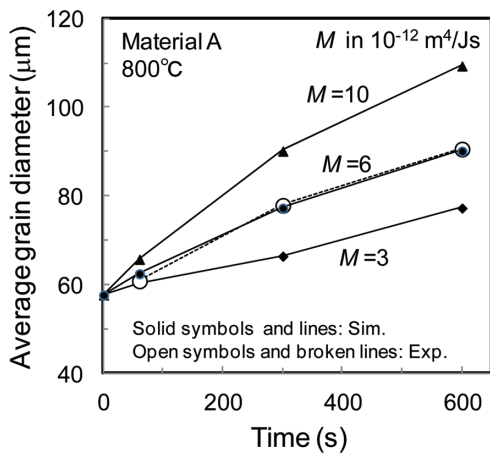


Fig. 2 Effect of grain boundary mobility on the average grain diameters

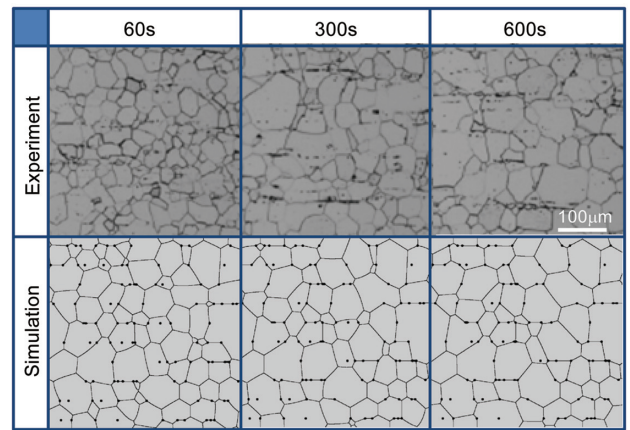


Fig. 4 Temporal evolution of the microstructure for Material B at 800°C (comparison of the experiments and the simulation)

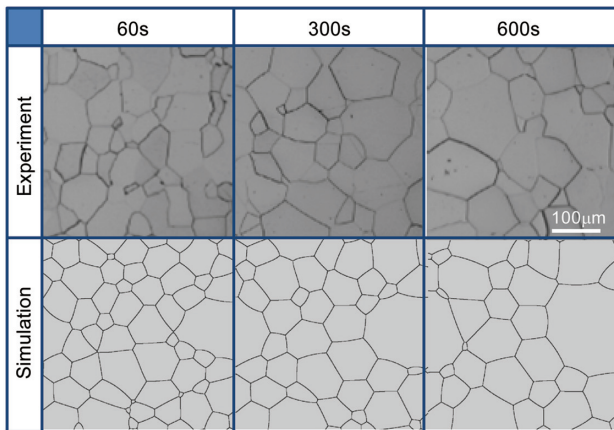


Fig. 3 Temporal evolution of the microstructure for Material A at 800°C (comparison of the experiments and the simulation)

mation calculation. As the  $\alpha$ -grain boundary mobility, the value obtained for Material A was used. It is considered that the amount and initial position of  $\beta$  grains significantly influence the growth behavior of  $\alpha$  grains. The volume % of  $\beta$  phase was assumed to be 1% based on the result of a calculation using Thermo-Calc. The initial size and distribution of  $\beta$  grains were decided with reference to photos of the microstructure. With the initial  $\beta$  grain size assumed to be  $4 \mu\text{m} \times 4 \mu\text{m}$  (or  $8 \times 8$  meshes),  $\beta$  grains were distributed preferentially within  $\alpha$ -grain boundaries.

Simulated microstructures of Material B and photos of the same are shown in Fig. 4. By comparing Fig. 4 with Fig. 3, it can be seen that the growth of  $\alpha$  grains in the  $(\alpha + \beta)$  region of Material B was suppressed by the presence of  $\beta$  phase. It can also be seen that  $\beta$  grains indicated by black spots in Fig. 4 are found on  $\alpha$  grain boundaries. This suggests that  $\beta$  grains had the pinning effect on  $\alpha$  grains. Figure 5 shows the simulated temporal evolution of grain size of Materials A and B, together with the experimental results. The simulation results agree well with the experimental results.

#### 4. Growth in Austenite Grains of SUS301L and SUS304

We carried out a simulation of the growth of grains in Nb-added austenitic stainless steel SUS301L.<sup>2,3)</sup> In the case of austenitic ( $\gamma$ )

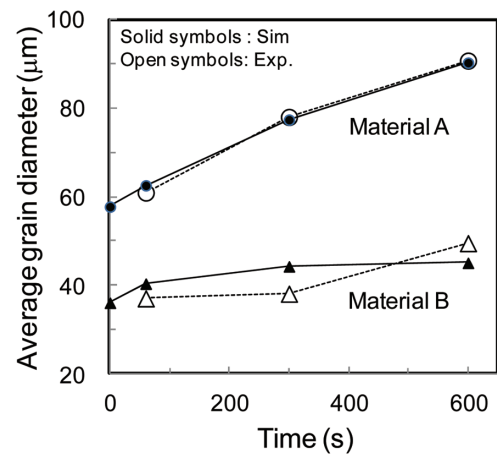


Fig. 5 Average grain size evolution for Material A and Material B at 800°C

stainless steels, grain refining is an effective method for increasing strength without decreasing ductility. There are various methods of refining grains of  $\gamma$  stainless steels.<sup>19)</sup> For SUS301L, in particular, the growth of grains is restrained by suppressed fine Nb(C, N) particles about tens of nm in size to precipitate. We examined the behavior of grain growth not only in SUS301L but also in SUS304 without Nb(C, N) precipitates. Using MICRESS,<sup>20)</sup> i.e., software for simulation with the multiphase-field method publicly available, we also studied the influence of the pinning effect of precipitates on the growth of grains within grain boundaries.

##### 4.1 Experimental

We carried out an experiment using two types of austenitic stainless steel. Their chemical compositions are shown in Table 2. The sample of SUS301L is added with Nb and precipitates fine particles of Nb(C, N).<sup>3)</sup> On the other hand, the sample of SUS304 is free of such fine precipitates. Therefore, SUS304 was used as a reference having no pinning particles. Each sample is a 0.4-mm-thick cold-rolled sheet obtained by subjecting a 5-mm-thick plate (obtained by hot-rolling a 17-kg vacuum-melted flat slab) to heat treatment, intermediate cold-rolling, solution heat treatment, and final cold-rolling. The cold-rolled sheet was then subjected to the final heat treatment at 900°C, 1,000°C, and 1,100°C for 30, 120, and 480 seconds, respectively. The final heat treatment represents the process of austen-

Table 2 Chemical compositions of samples used for the grain growth experiments of austenitic stainless steels

Sample	C	Cr	Ni	Si	Mn	Cu	Mo	N	Nb	Fe	Nb(C,N) precipitation
SUS304	0.05	18.1	8.1	0.5	0.8	0.25	0.25	0.045	0	Balance	–
SUS301L	0.02	17.2	6.6	0.5	1.4	0.25	0.25	0.012	0.05	Balance	Observed

ite grain growth. After heat treatment, the grain sizes in terms of diameter were calculated from photos of the microstructure under an optical microscope. The precipitates were too small (up to tens of nanometers) to observe under an optical microscope.

4.2 Method of simulation

MICRESS, which was used for the simulations, is capable of simulating the growth of grains on a mesoscale of single phase without considering the sample chemical composition.<sup>9,20</sup> When the pinning effect of dispersed particles is neglected, the only physical parameters to be input are the interface (grain boundary) mobility and the interface (grain boundary) energy. The influences of chemical composition and temperature are fully reflected in the value of interface mobility  $M$ . When consideration is given to the pinning effect of dispersed particles, the effective interface mobility,  $M_{eff}$ , defined by the following equation is used.<sup>9</sup>

$$M_{eff} = M \exp\left(\frac{-0.12p^*}{|\Delta G| - p^*}\right)$$

for  $|\Delta G| > p^*$ ,  $M_{eff} = M_{min} \ll M$  else , (5)

where  $p^*$  denotes the pinning force.<sup>13</sup> Equation (5) expresses that the driving force,  $\Delta G$ , for the growth of grains is substantially decreased by pinning force  $p^*$  and as a result, the interface mobility decreases. With MICRESS, quantity  $\kappa$  defined by the following equation is used as the pinning parameter.

$$\kappa \equiv p^* / \sigma . \quad (6)$$

The unit of  $\kappa$  is the reciprocal of length.

The calculation region was  $200 \mu\text{m} \times 200 \mu\text{m}$ , the mesh size was  $0.5 \mu\text{m}$ , and the number of meshes was  $400 \times 400$ . The grain boundary energy was assumed to be  $1 \text{ J/m}^2$ . The interface mobility and the pinning parameter were treated as fitting parameters, which were so adjusted that the average  $\gamma$  grain size would coincide with the experimental value. The initial grain size in the simulation was made the same as the average  $\gamma$  grain size for 30 s obtained in the experiment. With both types of stainless steel, the  $\gamma$  grain size at  $900^\circ\text{C} \times 30 \text{ s}$  was so small that it could not be measured. Therefore, at  $900^\circ\text{C}$ , the simulation was started using the measured grain size for 120 s as the initial grain size.

4.3 Interface mobility

The interface mobility was decided by simulating SUS304, which is entirely of  $\gamma$  phase and that has no pinning effect of precipitates. Namely, we repeated a simulation in which the values of grain boundary mobility was varied such that the average  $\gamma$  grain sizes obtained by the experiment under the different conditions would coincide with those obtained by the simulation. Figure 6 shows an Arrhenius plot displaying the product of interface mobility  $M$ , decided at each temperature by the above simulation, and temperature  $T$ . The linearity of the plot indicates that the model expressed by Equation (3) is valid. Figure 7 shows the temporal evolution of average  $\gamma$ -grain size at each of the different temperatures, calculated by using the above interface mobility together with the experimental re-

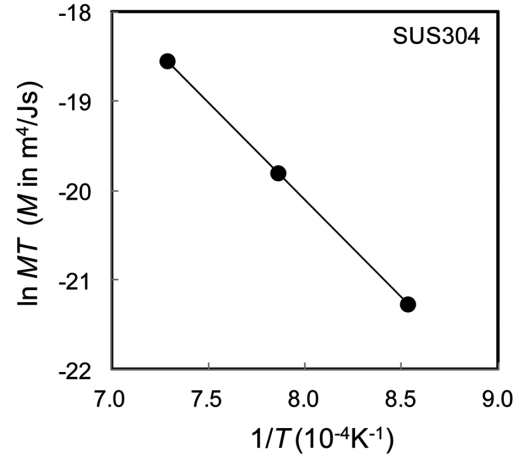


Fig. 6 Relation between the grain boundary mobility and temperature for SUS304

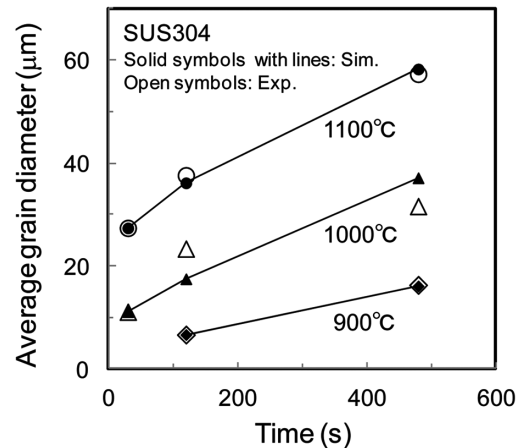


Fig. 7 Average grain size evolution for SUS304 (comparison of the experiments and the simulation)

sults. Thus, by adjusting properly the parameter of boundary motion, it is possible to make the calculated grain size almost coincide with the experimental value.

4.4 Pinning parameter

In the SUS301L sample, Nb(C, N), which is finely precipitated, serves as pinning particles.<sup>3</sup> We carried out a simulation using the pinning parameter, defined by Equation (6), as the fitting parameter. As the interface mobility, the value decided on the basis of experimental results obtained with SUS304 was directly used. For each of the different simulation temperatures, the pinning parameter was varied such that the average  $\gamma$  grain size calculated would coincide with the experimental value. Figure 8 shows the relationship between pinning parameter  $\kappa$  and temperature obtained by the above simulation. The value of  $\kappa$  begins to decrease sharply at  $1,100^\circ\text{C}$ , in-

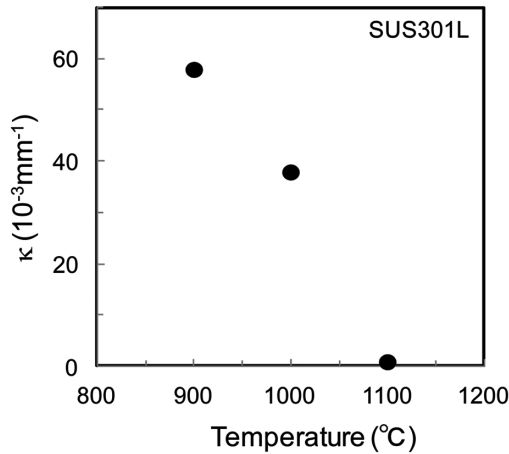


Fig. 8 Relation between the pinning parameter  $\kappa$  and temperature for SUS301L

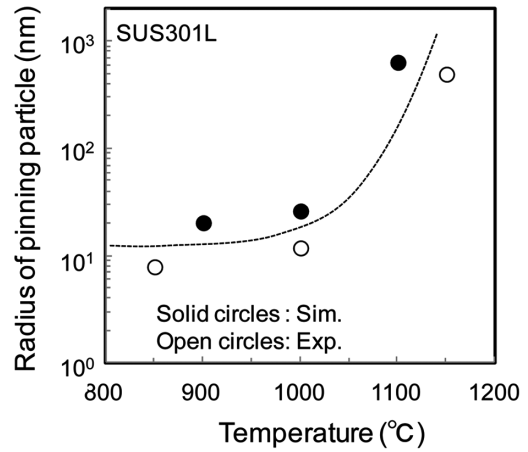


Fig. 10 Relation between the radius of pinning particles and temperature calculated from  $\kappa$  for SUS301L

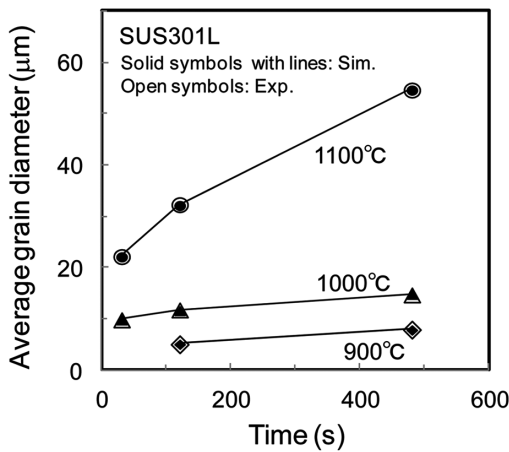


Fig. 9 Average grain size evolution for SUS301L (comparison of the experiments and the simulation)

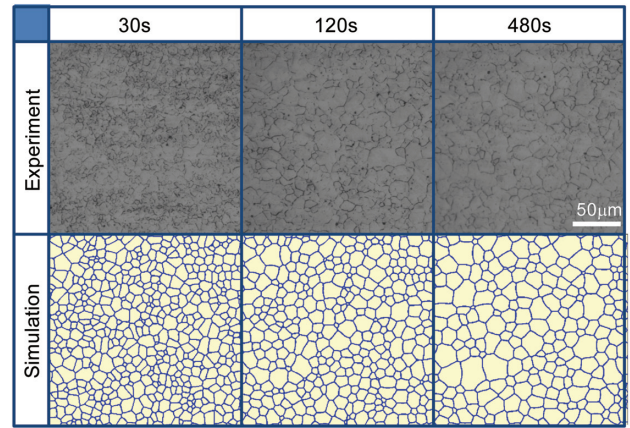


Fig. 11 Temporal evolution of the microstructure for SUS301L at 1,000°C (comparison of the experiments and the simulation)

dicating that the pinning effect of precipitates declines markedly at that temperature. The implication is that the amount, size, distribution, etc. of fine precipitates change rapidly. **Figure 9** shows the temporal evolution of average grain size at each of the different temperatures, obtained by the simulation using the above pinning parameters, together with the experimental results. As shown, the accuracy of fitting with the experimental values is very high. From Figs. 7 and 9, it can be seen that the grain size decreases at 900°C and 1,000°C, respectively, because of the pinning effect.

#### 4.5 Size of pinning particles

The particles of Nb(C, N) were too small to observe under an optical microscope. Therefore, we estimated the radius of pinning particles using Equation (6), which gives a pinning parameter for MICRESS. For pinning force  $p^*$  in Equation (6), several models have been proposed. Here, the pinning model<sup>13)</sup> of Zener–Smith shown below is used.

$$p^* = \frac{3}{2} \cdot \frac{\sigma f}{r_{pin}}, \quad (7)$$

where  $f$  denotes the volume fraction of dispersed particles and  $r_{pin}$  denotes the average radius of dispersed particles.

From Equations (6) and (7), the following equation can be de-

rived.

$$r_{pin} = \frac{3}{2} \cdot \frac{f}{\kappa}. \quad (8)$$

Thus, the radius of dispersed particles can be estimated from  $\kappa$  and  $f$ . For  $f$ , the values obtained by Thermo-Calc were used. They were  $7.98 \times 10^{-4}$  at 900°C,  $6.71 \times 10^{-4}$  at 1,000°C, and  $4.30 \times 10^{-4}$  at 1,100°C. **Figure 10** shows the relationship between  $r_{pin}$  and temperature, obtained by substituting those values of  $f$  in Equation (8). As shown in Fig. 10, the particles of Nb(C, N) became coarse markedly at 1,100°C. Fig. 10 also shows the radii of Nb(C, N) particles observed under a transmission electron microscope.<sup>3)</sup> The calculated values agree well with those measured values. **Figure 11** compares the microstructures obtained by the simulation with those obtained by the experiment. They are very similar to each other.

## 5. Conclusion

To establish a technique for predicting the grain sizes of metallic materials, we simulated the growth of grains in titanium and stainless steels using the phase-field model.

In the simulation of the growth of  $\alpha$  grains in commercially pure titanium sheet, the results of the experiment on the pinning effect of  $\beta$  grains on the growth of  $\alpha$  grains could be qualitatively explained

through a simulation taking the  $\beta$  phase into consideration.

In the simulation of the growth of  $\gamma$  grains in austenitic stainless steel SUS301L with fine Nb(C, N) precipitations, we could measure the pinning effect of fine Nb(C, N) particles using a suitable parameter and estimated the average size of Nb(C, N) particles from the simulation results.

In each simulation, the average grain size obtained by the experiment could be accurately reproduced by means of parameter fitting. The interface mobility obtained by fitting and the value of pinning parameter have physical meaning, so that once decided, they can be applied in simulations of other titanium alloys and stainless steels.

#### Acknowledgments

The author thanks Mr. Jin Jonghoon, summer intern (August 2012) from the Tokyo Institute of Technology, for his cooperation in our simulations.

#### References

- 1) Adachi, K., Nakayama, E., Shibuya, M., Fukumura, Y., Fujisawa, K., Kurita, A.: Development of Stainless Steel Sheets for Cylinder Head Gasket. Shinnittetsu Sumikin Giho. (396), 92 (2013)
- 2) Sawada, M., Kita, H., Shibuya, M., Fujisawa, K.: Development of Austenitic Stainless Steel Plate for Precision Working. Shinnittetsu Sumikin Giho. (396), 85 (2013)
- 3) Sawada, M., Adachi, K., Maeda, T.: ISIJ Int. 51, 991 (2011)
- 4) The Iron and Steel Institute of Japan (ISIJ): 161st–162nd Nishiyama Memorial Technical Lecture “Technology for Controlling Microstructures of Steel and Titanium”. Tokyo, ISIJ, 1996
- 5) Takaki, T., Yamanaka, A.: Phase-Field Method. Tokyo, Yokendo, 2012
- 6) Raabe, D.: Computational Materials Science. Weinheim, Wiley-VCH, 1998
- 7) Moelans, N., Blanpain, B., Wollants, P.: Acta Mater. 54, 1175 (2006)
- 8) Suwa, Y.: Grain Growth Simulation Using Phase-Field Method. Shinnittetsu Giho. (392), 19 (2012)
- 9) Apel, M., Bottger, B., Rudnizki, J., Schaffnit, P., Steinbach, I.: ISIJ Int. 49, 1024 (2009)
- 10) Steinbach, I., Pezzolla, F., Nestler, B., Seesselberg, M., Prieler, R., Schmitz, G.J., Rezende, J.L.L.: Physica D. 94, 135 (1996)
- 11) Saunders, N., Miodownik, A.P.: CALPHAD: A Comprehensive Guide. Elsevier, Oxford, 1998
- 12) Eiken, J., Bottger, B., Steinbach, I.: Phys. Rev. E. 73, 066122 (2006)
- 13) Nishizawa, Y.: Thermodynamics of Microstructures. ASM International, Materials Park, 2008
- 14) Thermo-Calc Software: <http://www.thermocalc.com>
- 15) Hillert, M.: Metall. Trans. A. 6A, 5 (1975)
- 16) Tiaden, J., Nestler, B., Diepers, H.J., Steinbach, I.: Physica D. 115, 73 (1998)
- 17) Seki, A., Moriguchi, K., Shirai, Y., Maeda, T.: CAMP-ISIJ. 24, 421 (2011)
- 18) ISIJ Subcommittee for the Study of Heat-Resistant Tough Titanium—Physical Properties WG: Data about Dispersions in Titanium/Titanium Alloys, 1994
- 19) Takaki, S.: Bulletin of ISIJ. 16, 550 (2011)
- 20) MICRESS: <http://www.micress.de>



Akira SEKI  
Senior Researcher, Dr.Eng.  
Titanium & Specialty Stainless Steel Research Lab.  
Steel Research Laboratories  
1-8 Fuso-cho, Amagasaki City, Hyogo Pref. 660-0891



Masayoshi SAWADA  
Researcher  
Titanium & Specialty Stainless Steel Research Lab.  
Steel Research Laboratories



Koji MORIGUCHI  
Senior Researcher, Dr.Eng.  
Pipe & Tube Research Lab.  
Steel Research Laboratories



Yoshihisa SHIRAI  
Senior Researcher  
Titanium & Specialty Stainless Steel Research Lab.  
Steel Research Laboratories